JOURNAL OF Applied Polymer SCIENCE

Examination of radio-opacity enhancing additives in shape memory polyurethane foams

Andrew C. Weems,[1] Jeffery E. Raymond,[2] Kevin T. Wacker,[3,4,5] Tiffany P. Gustafson,[2] Brandis Keller,[1] Karen L. Wooley,[2,3,4,5] Duncan J. Maitland[1]

[1]Department of Biomedical Engineering, Biomedical Device Laboratory, Texas A&M University, Texas 77843-3120
[2]Department of Chemistry, Laboratory for Synthetic-Biologic Interactions, Texas A&M University, Texas 77843-3120
[3]Department of Chemistry, Texas A&M University, Texas 77843-3120
[4]Department of Chemical Engineering, Texas A&M University, Texas 77843-3120
[5]Department of Materials Science and Engineering, Texas A&M University, Texas 77843-3120
Correspondence to: D.J. Maitland (E-mail: djmaitland@bme.tamu.edu)

ABSTRACT: Three microparticle additives, tungsten (W), zirconium oxide (ZrO_2), and barium sulfate ($BaSO_4$) were selected to enhance the radio-opacity in shape memory polymer (SMP) foam biomaterials. The addition of filler causes no significant alterations of glass transition temperatures, density of the materials increases, pore diameter decreases, and total volume recovery decreases from approximately 70 times in unfilled foams to 20 times (4% W and 10% ZrO_2). The addition of W increases time to recovery; ZrO_2 causes little variation in time to shape recovery; $BaSO_4$ increases the time to recovery. On a 2.00 mean X-ray density (mean X.D.) scale, a GDC coil standard has a mean X.D. of 0.62; 4% W enhances the mean X.D. to 1.89, 10% ZrO_2 to 1.39 and 4% $BaSO_4$ to 0.74. Radio-opacity enhancing additives could be used to produce SMP foams with controlled shape memory kinetics, low density, and enhanced X-ray opacity for medical materials. © 2015 Wiley Periodicals, Inc. J. Appl. Polym. Sci. **2015**, *132*, 42054.

KEYWORDS: biomaterials; foams; polyurethanes; stimuli-sensitive polymers; X-ray

Received 29 September 2014; accepted 26 January 2015
DOI: 10.1002/app.42054

INTRODUCTION

The high recovery strain and large reversible changes in elastic moduli during the transition between glassy and rubbery phases have made shape memory polymers (SMPs) appealing for a wide variety of medical devices, such as vascular grafts, stents, coronary implants, orthopedic braces, and splints; SMPs also provide advantages over shape memory alloys.[1–4] Wilson *et al.* and Singhal *et al.* presented a SMP thermoset polyurethane system that demonstrated exceptional shape memory behavior, with controlled glass transition temperature (T_g) of approximately 80°C, mechanical behavior, and biocompatibility. *In vivo* studies by Rodriguez *et al.*[5] have shown less inflammation in surrounding tissue compared with FDA approved sutures, and ingrowth fibrin and collagen throughout the foam matrix when implanted for 30 and 90 day studies.

A major drawback for polyurethanes is the lack of radio-opacity, which is insufficient to be seen using clinical fluoroscopic imaging equipment, and is a limitation for materials used in medical devices. By comparison, endovascular devices such as Guglielmi detachable coils (GDC coils) used in aneurysm occlusion possess sufficient radio-opacity to appear on standard clinical imaging equipment.[6–10]

In this study, the radio-opacity enhancing moieties tungsten (W), barium sulfate ($BaSO_4$), and zirconium oxide (ZrO_2) were physically added to SMP foams.[2,11–32] The usage of these materials in medical device applications is briefly mentioned below. To our knowledge, this is the first reported use of SMP foams with ZrO_2 and $BaSO_4$ additives.

Previous work by our group has examined both the opacity and compatibility of tungsten (W) used in SMP foams, showing that 4% W loading dramatically increased opacity in clinical imaging while maintaining good tissue compatibility/healing over a 90-day examination.[11] However, the shape recovery properties and kinetics of W filled foams were not examined. W has been used in embolization devices in the form of embolic coils with degradation products being below cytotoxic limits.[12–16]

In medical procedures, $BaSO_4$ is used for imaging contrast procedures, and to enhance opacity in dental adhesives and vascular devices, even at low concentrations (~1.0%) when impregnated in solid polymers.[2,17–25] Romero-Ibarra *et al.* and

Cui *et al.*[26–28] demonstrated full shape recovery using $BaSO_4$ at 40% loading by weight, indicating that high concentrations of additives would not drastically alter the volume recovery.[26,27] Additionally, $BaSO_4$ has been directly injected in the bloodstream due to errors during gastrointestinal imaging without long-term complications, and leaches from doped catheters used in vascular applications.[23,24,28]

A literature search revealed some attempts at using ZrO_2 in dental applications to better image adhesives.[18,19,29] ZrO_2 has been shown to have better cytocompatibility than polyethylene, and has been used in orthopedic applications such as femoral head coatings in total hip replacement devices, with data showing a lower inflammatory response compared to titanium when implanted.[30–33] ZrO_2-coated surfaces also possess hemocompatibility with decreased time to thrombus formation compared with uncoated surfaces or stainless steel, and could be used for a blood contacting device without inducing toxicity.[34–37] Since the material is oxidized, there is little chance of leaching from the bulk material into the surrounding tissue or blood stream.

For SMP foams with additives, the target polymer matrix would possess sufficient porosity, kinetics, and mechanical properties for use in medical devices while maintaining enhanced radio-opacity. An ideal SMP system would make use of tailored pore sizes in the foam, have a well understood, application-selected thermo-mechanical set of properties, controlled recovery kinetics, and enhanced optical properties. Herein, we show that additives, reported to improve radio-opacity in medical applications, can be used to decrease pore size, increase density, alter shape recovery kinetics, and enhance X-ray density in order to develop a SMP system for biomaterials and medical devices.

EXPERIMENTAL

Materials

N,N,N′,N′-Tetrakis(2-hydroxypropyl)ethylenediamine (HPED, 99%, Sigma Aldrich), triethanolamine (TEA, 98%, Sigma Aldrich) and 2,2,4-trimethyl hexamethylene diisocyanate (TMHDI, TCI America, a mixture of 2, 2, 4 and 2, 4, 4 monomers) were the monomers used in the synthesis. $BaSO_4$ (particle size of 3 μm, 99%, Sigma Aldrich), ZrO_2 (particle size of 5 μm, 99%, Sigma Aldrich), and W (particle size >1 μm, 99.95%, Alfa Aesar) were used as additives. Both the monomers and the additives were used without modification.

Foam Synthesis

SMP thermoset foams were made using the compositions reported by Wilson *et al.*[3] These three monomers were reacted to form a prepolymer mix, which underwent a heating cycle of 6 h at room temperature, a ramp of 20°C/h to 50°C, held at 50°C for 16 h and then was allowed to cool to room temperature and set in a nitrogen chamber until used. The prepolymer mixture was made 2 days before foaming, allowing for 100 : 40 ratios of isocyanates to alcohols to form a network. Second, an alcohol premix containing alcohols, surfactants and catalysts in stoichiometric amounts was made. The final step was the combination of both premixes along with the one of the additive species and physical blowing agents using high speed mixing to synthesize homogeneous foams. The examined concentrations of additives in 16 g foam are 1% (0.831 g $BaSO_4$, 0.907 g for ZrO_2, and 3.554 g for W) and 4% (3.324 g $BaSO_4$, 3.626 g for ZrO_2, and 14.218g for W) compositions by volume (as well as 10% for ZrO_2). Particle dispersion in the foams was examined using scanning electron microscopy (SEM). A Vega3 Tecscan SEM, using 15.0 kV power and an initial sample distance and 15 mm. Magnification of 112× was examined using both backscattering and secondary scattering, and 332× using backscattering; the sample distance was varied from 15 mm to give the best images. The density of the foams was dependent on the gas concentration in the foam during synthesis, and thus the amounts of surfactants, catalysts, physical and chemical blowing agent were varied to ensure the maximum effective concentration of gas without causing cell rupture. The foam was evaluated for homogeneous pores before cleaning and processing. After cleaning, foams were dried and stored with desiccant in a sealed container.

Density

Density measurements were taken following ASTM standard D-3574-08 procedure. Sample measurements were taken across the diameter of the synthesized foam in order to give an average density for the usable portion of the foam. This section was defined as the portion of foam that contained uniform pores, both in size and morphology, when visually inspected.[4]

Thermal Characterization

Differential scanning calorimetry (DSC) using a Q200 TA DSC with a TA Refrigerated Cooling System 90 (TA Instruments, New Castle, DE) was performed on samples approximately 4.0 mg ± 1.0 mg. The samples were sealed in TA Tzero aluminum hermetic pans at room temperature and inserted immediately into the test cell. Dry samples were equilibrated at −40°C for 5 min before going through a heat-cool-heat cycle to 120°C at 10°C/min. The half-height transition point in the third heating cycle was recorded as the dry T_g.

Samples containing approximately 1.0 mg of DI water were sealed in Tzero pans at ambient conditions and placed in the testing cell. The samples were equilibrated at −40°C for 5 min and then ramped to 80°C at 10°C/min. The inflection point of the heat flow profile was taken as the wet T_g. Five samples for both wet and dry experiments were examined.

Thermal analysis via dynamic mechanical analysis (DMA) was performed using a Q800 TA DMA (TA Instruments, New Castle, DE) for dry samples, and a TT-DMA (Mettler-Toledo AG, Schwerzenbach, Switzerland) for both immersion kinetics and wet temperature sweeps. Foam cylinders 6 mm in diameter and 5 mm in length were axially compressed to 0.8 mm. The samples were allowed to equilibrate at 100°C for 10 min before compression and were then cooled to room temperature under compression.

Dry temperature sweep samples were equilibrated at 20°C for 15 min, and then ramped to 120°C at a rate of 3°C/min. The storage modulus (E') and the loss modulus (E'') were used to determine the tan δ (E'/E''), with the maximum value recorded as the dry T_g.[38]

The effect of plasticizer on T_g is crucial in medical devices, as polyurethanes have been shown to demonstrate a lower

apparent T_g.[38–40] To determine the wet T_g, samples were immersed in PBS solution and equilibrated for 5 min at 25°C. The solution was ramped at a rate of 1°C/min manually to 70°C. The temperature corresponding to the peak of the tan δ curve was recorded as the wet T_g.[38] Four samples were examined.

Samples of approximately 7 mg were examined using a Mettler Toledo thermogravimetric analyzer (TGA)/DSC 1. The samples were weighed and heated from room temperature to 600°C at a rate of 10°C/min under argon atmosphere. Onset temperature of degradation (inflection point) and slope were compared using Mettler-Toledo v.10.00 Star[e] software.

Pore Sizes

Thinly sliced foam strips were cut using a hot wire cutter. Using a metric ruler as a standard, the pore images were taken using Leica M716 confocal microscope (JH Technologies, Inc., Silicon Valley) in brightfield mode with a Jenoptic camera (Laser Optik Systeme GmbH, Germany) attached. RS Image Software (Roper Scientific, Tucson, AZ) was used for image capturing, and processing was performed with Image J software (National Institute of Health, Washington, DC). The pore sizes were calculated for both the long and short diameters, averaged across three foam samples of each series, with twenty pores measured in each.

Volume Recovery

The maximum volume recovery of the foam samples was determined using a SC150-42 Stent Crimper (Machine Solutions, Flagstaff, AZ). Cylindrical foam samples (6mm in diameter and 10 mm long, six samples per series), at 100°C, were radially compressed as much as possible along a length of wire, and cooled to room temperature. Allowing for 12 h of relaxation before testing, the samples were placed in a water bath at 70°C. Images were taken before crimping, after crimping, and at select increments during the 10 min immersion for six samples of each species, with nine measurements for each sample used for standard deviation calculation. Images were analyzed using Image J software to determine the total volume recovery, which is calculated by eq. (1)

$$\text{Volume}_{\text{recovered}} = \left(\frac{\text{Diameter}_{\text{expanded}}}{\text{Diameter}_{\text{crimped}}}\right)^2 \quad (1)$$

Since length is assumed constant for these samples, the change in diameter is the change in the volume of the sample. Equation (2) shows how this metric compares to strain recovery, a more common metric

$$\text{Strain recovery} = \frac{R_{\text{expanded diameter}}}{R_{\text{initial diameter}}} \times 100 \quad (2)$$

Volume recovery at 50°C was also examined, to determine the behavior of the materials when utilized in device applications. The samples were crimped using the methods described above, and allowed to relax for 12 h after shape setting. Samples were immersed in 50°C DI water for 30 min, with images taken every 30 s. Image J was used to determine the volume recovery over the course of the trials. Six samples of each species were examined, with nine measurements taken from each sample to calculate standard deviation.

As mentioned in the Thermal Characterization section, immersion kinetics of shape recovery were also examined using the environmental DMA. The examined foam geometry was the same as for wet temperature sweeps. Samples were placed between the compression plates and then immersed in 50°C PBS solution. E' was shown to vary over the course of the immersion; E'_{max}, the maximum modulus value recorded, was used as a metric for comparison, as was E'_{final}, which was determined using a straight line approximation of the modulus plateau. These metrics were averaged over the four examined samples.

Radio-Opacity Determination

Foam samples of 6 mm in diameter and approximately 3 cm long were compressed along monofilament line, and stretched in a custom frame. A GDC coil and a custom Pt coil were used as standards, and were placed in the frame.

X-ray images were acquired on a Bruker In-Vivo Xtreme multimodal preclinical imaging system (Bruker BioSpin Corp.) outfitted with a 4 MP back-thinned, back-illuminated 4MP CCD detector. X-rays were collected with an exposure time of 1.0 s, where the *f*-stop = 1.40, FOV = 153.0 mm, vertical and horizontal resolution = 377 ppi and X-ray energy = 45 KVP. Images were edited using Bruker molecular imaging software. The background was subtracted using an illumination correction reference obtained under the same conditions. To quantify the radio-opacity for each material, a length of 0.48 cm was selected along each material in the X-ray image as the region of interest. 68 samples of X-ray density (X.D.) were taken within the region of interest utilizing Bruker Molecular Imaging Software. From these measurements, a mean and standard deviation of the X.D. were calculated.

RESULTS AND DISCUSSION

Material Characterization

Loading concentration is a limitation for additives in SMP foams, with higher loading resulting in collapsed foams or nonhomogeneous pores. For the W and $BaSO_4$ series, this was limited to approximately 4%. The ZrO_2 series had a loading limit of approximately 10%. SEM imaging showed clumping of microparticles in all samples. 1% additives appeared to have less particle aggregation compared with higher loadings. As shown in Table I, the density of unfilled foams was approximately 0.0125 g/cc, a characteristic first reported by Singhal *et al.*[4,40] The increase in density will be caused in part by the additional weight of the filler material; changes in the morphology resulting from the presence of additives also occurred, and may be the cause of the increased density.

The dry and wet T_g values obtained by DSC and DMA are shown in Table I. DSC dry samples had a T_g of approximately 74°C when unfilled, with increasing additive concentration decreasing the T_g values, or showing no change. Wet samples showed a tighter clustering of T_g, approximately 30°C lower than dry samples. DMA of the materials also showed no significant deviation in the T_g, with all dry samples having maximum tan δ around 90°C. Transitions in the peak did not follow any trend. Immersed samples showed peaks at approximately 56°C for samples compressed and tested within 24 h. The small variation of both dry and wet peak values indicates that the presence

Table I. Average Density and Thermal/Mechanical Transitions of SMP Foams with Additives

Foam composition	Density (g/cc)	Dry T_g (DSC) (°C)	Wet T_g (DSC) (°C)	Dry tan δ max (°C)	Wet tan δ max (°C)
Unfilled foam	0.0124 ± 0.0002	74.0	47.8	89.1	57.0
1% $BaSO_4$	0.0120 ± 0.0004	71.1	44.0	90.8	57.2
4% $BaSO_4$	0.0231 ± 0.0011	69.3	44.5	89.0	54.7
1% W	0.0162 ± 0.0015	70.8	45.7	94.4	57.8
4% W	0.0766 ± 0.0056	65.8	45.0	88.7	57.5
1% ZrO_2	0.0128 ± 0.0004	73.5	45.8	91.0	55.1
4% ZnO_2	0.0162 ± 0.0010	68.8	47.2	89.8	54.9
10% ZnO_2	0.0405 ± 0.0028	67.8	46.0	90.1	55.2

of additives in the foams does not significantly alter the temperatures of use for the material, which would be a crucial consideration for inclusion in medical devices. Other studies have shown SMP composites demonstrating reduced T_gs, which could be due to particle size (nanoscale), with sufficiently small particles disrupting crosslinking, and in some cases sufficiently high loading concentrations in addition to being affected by aggregation.[27,28,41] An important note is that the measured T_g for the wet samples was below 60°C, which would allow for use in medical devices. Above 60°C, collagen begins to denature, and below 37°C the materials would begin to actuate passively due to body heat.[42–45] TGA data showed a degradation onset temperature of approximately 230°C ± 10°C for all samples, with the same slopes. The only variation was with the remaining mass, dependent on the filler species and loading concentrations.

Unfilled polyurethane foam [Figure 1(A)] was found to have the largest pores, determined by measuring the longest diameter and the perpendicular diameter. The analysis shown in Figure 1 takes the average of two diameters of the pores. With greater concentrations of additives [Figure 1(B–D)], the difference in the pore diameters decreased, shown by the decreasing standard deviation error bars. Previous studies have shown that particle inclusion can alter pore size and disrupt pore morphology, depending on particle species and loading concentrations.[46–48]

Shape Recovery Characterization

In order to determine the actuation kinetics, immersion DMA was used to examine material behavior at wet T_g, as determined by DMA. As the concentration of W increased, the time to the modulus peak (E_{max}) increased [shown in Figure 2(A)]. Comparison of the moduli was done after normalization using the maximum modulus value, shown in Table II, for each individual species. The time to E_{max} was approximately 2.5 min for unfilled SMP foams, and shifted to approximately 5.5 min for 4% W, as determined from the curve fittings of these data sets. This shows an increasing time to expansion with increasing concentration for the W series.

The graph of the tan δ versus time of the W series, where the inflection point of the sample indicates the time at which the material undergoes a transition from a more elastic sample to a more viscous one, is shown in Figure 2(B). The time to the inflection point increases with increasing concentrations of W filler. The phase transition point for the series (the inflection point) occurs at approximately 10 min, and shifts to nearly 20 min for 4% W SMP foams.

Materials containing 1% ZrO_2 and 10% ZrO_2 filler demonstrated a shifted E_{max} slightly, to longer times, but for those containing 4% ZrO_2, the E_{max} peak occurred approximately at the same time as for the unfilled foam. The phase transition trend shows that while the 1% ZrO_2 increased the phase transition time from approximately 6.1 min to 12.0 min, the 4% ZrO_2 and 10% ZrO_2 filler only increased time to the phase transition relative to unfilled foam. The behavior of the 10% ZrO_2 material did not have a uniform transition similar to any of the lower loading concentrations examined.

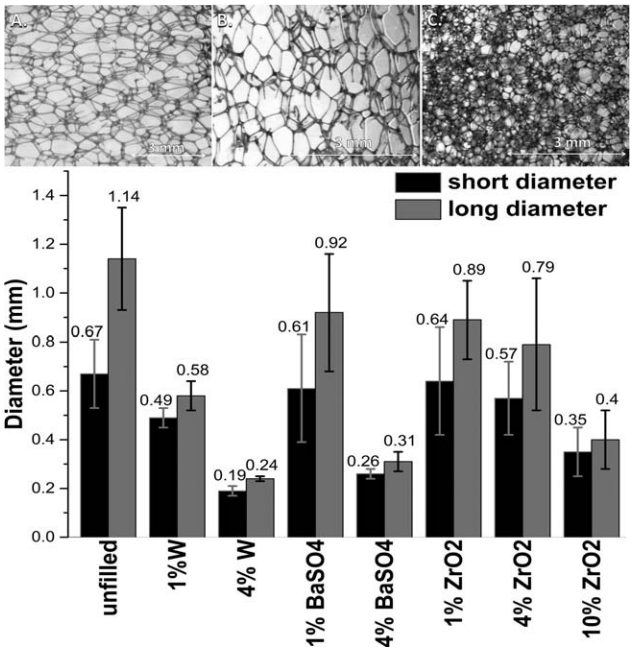

Figure 1. Above, confocal microscopy of (A) unfilled foam pores, (B) 1% W and (C) 4% W filled foam pores. Below, the average foam pore diameter based upon loading species and concentration. The pores were treated as two-dimensional entities, with two perpendicular diameters of the pores being used to calculate the diameter of the pore. The average diameter is shown above the error bars ($n = 20$).

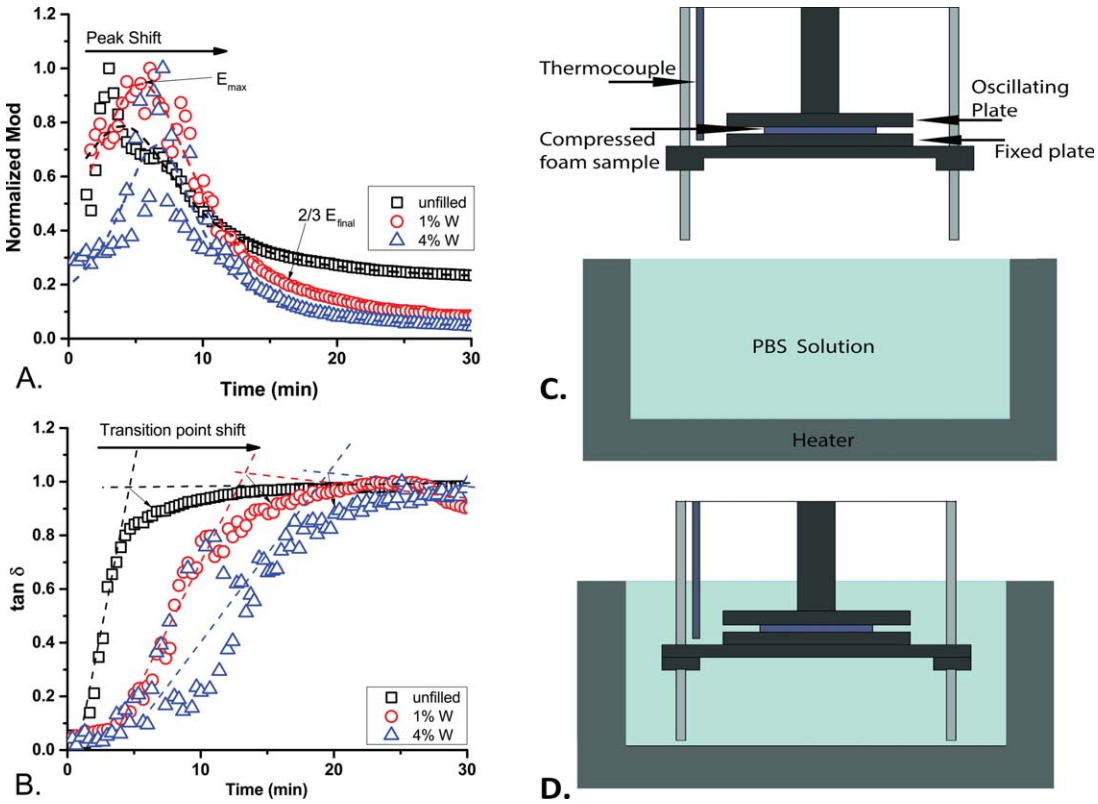

Figure 2. The immersion DMA over time representative curves, showing the data for the W series, while immersed in 50°C PBS solution (A. normalized modulus, B. tan δ) ($n = 3$). The experimental apparatus is shown before immersion (C) and when immersed (D). [Color figure can be viewed in the online issue, which is available at wileyonlinelibrary.com.]

The behavior of the $BaSO_4$ fillers showed the E'_{max} peak shifted to the right for the 1% $BaSO_4$ loading, and the 4% $BaSO_4$ loading was between the unfilled and the 1% $BaSO_4$. This behavior was seen for the phase transition trends as well. $BaSO_4$ showed a distinct shift for loading compared with unfilled, but concentration of additive did not reveal a distinct behavior for concentrations examined.

Upon introduction of the SMP foam samples into the PBS, the moduli of the samples increased; the time to this maximum modulus is shown in Table II. The delay in actuation could be due to the microscopic reordering of the polymer chains before shape recovery beginning.[3] As demonstrated by Sauter *et al.*, in amorphous SMP polyurethane foams pore size distribution directly affects the shape recovery.[49,50] The smaller pores will decrease the influx rate of PBS into the entire material, which will decrease plasticization of the polymer chains. The slower plasticization will increase time until shape recovery begins, as seen in Figure 2.

Since the foam was compressed and dry before introduction to the solution, it was considered that the time to actuation was being increased due to a diffusion barrier provided by the testing apparatus geometry, shown in Figure 2(C). The solution

Table II. Expansion Metrics for Volume Recovery

Series	E_{max} (MPa)	E_{final} (MPa)	Time to E_{max} (min)	Time to expansion start (min)	Time to 2/3 E_{final} (min)	Time to 90% diameter (min)
Unfilled foam	0.480	0.225	2.20	2.31	17.61	18.84
1% $BaSO_4$	1.073	0.161	3.15	4.28	18.36	20.41
4% $BaSO_4$	2.198	0.170	3.37	3.97	18.45	16.41
1% W	5.413	0.143	2.60	2.63	25.02	23.42
4% W	17.987	0.124	5.10	4.71	30.25	28.05
1% ZrO_2	0.816	0.138	2.41	5.01	17.16	20.62
4% ZnO_2	9.798	0.058	2.58	2.76	13.39	24.79
10% ZnO_2	4.716	0.310	4.46	2.18	9.33	19.52

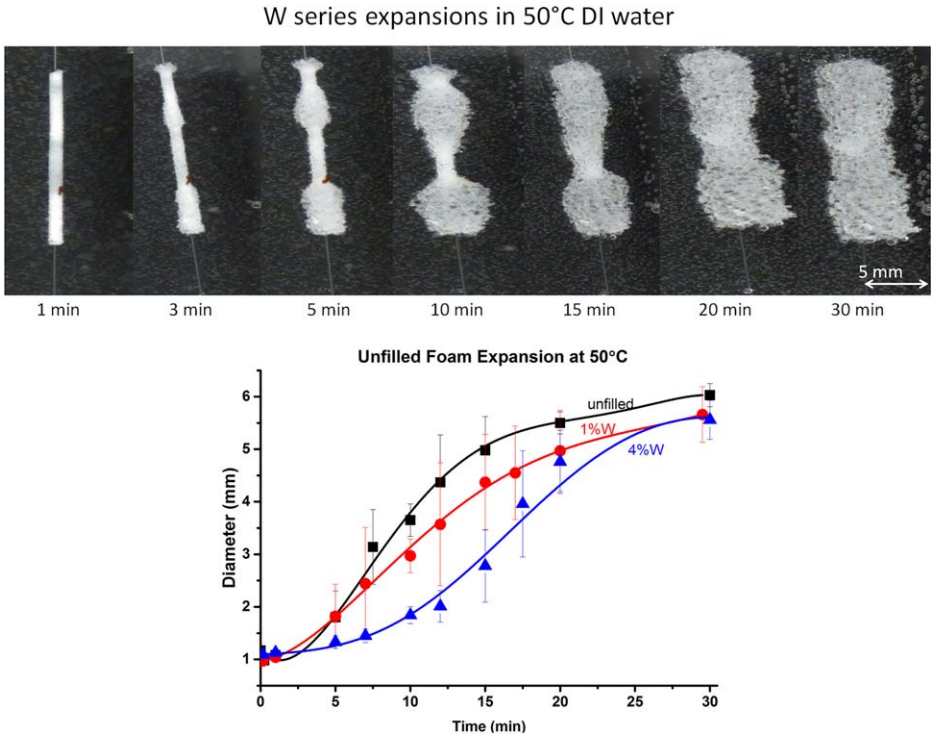

Figure 3. Above: the expansion bulk materials shown at various time steps. Below: expansion studies using bulk samples in 50°C DI water for the tungsten series. [Color figure can be viewed in the online issue, which is available at wileyonlinelibrary.com.]

would be limited in how quickly it could diffuse throughout the entire sample, increasing the time to bond plasticization and foam relaxation.

These potential diffusion limitations led to bulk material expansion studies as a method of decoupling geometry from shape recovery kinetics. Taking into account variability in image processing, 25% of the initial diameter was allowed for expansion before actuation was considered to have started. An example of the bulk material expansion is shown in Figure 3.

Expansions of unfilled foams occurred at approximately 1.5 min; 1% W expansion began at approximately 2.0 min; 4% W expansion began at approximately 3.5 min. Table II shows the metrics recorded for all examined series. The kinetics of the DMA expansion showed a similar trend, with the differences in the specific metrics explained by the error due to Image J analysis of the expansion images and averaging the trends of specific samples into behavior of the foam series. As can be seen by the top image in Figure 3, the unfilled foams show a fast expansion behavior that occurs until approximately 5.5 mm diameter, where the expansion becomes much slower as it approaches the final diameter. The 1% W (bottom left) behavior demonstrated similar trends, with the change shape recovery corresponding to the phase transition of the material. SMP foams with 4% W loading (bottom right) demonstrated three behavior regions, with the initial slow expansion becoming apparent and extended compared with unfilled and 1% W SMP foam. The rapid expansion occurred over a decreased time once actuation had started, and the final expansion occurred in approximately the final 0.5 cm of the volume recovery. This final expansion seemed to become the dominating expansion trend at approximately 90% of the final diameter, shown in Table II. Studies by Cui and Lendlein demonstrated two distinct shape recovery regimes, a fast process for the majority of the material, and a slow expansion for the final diameters at long times (>120 min).[27]

The expansion of the foams was affected by the crimping process. If the foams on the wire were touching before crimping, which could occur during the loading of the foams into the crimper, the crimped foam would be one long cylinder, rather than three short ones. The shape recovery of these two geometries is slightly different due to the surface area exposure to water during the expansion, with greater surface area showing faster kinetics. Foam relaxation after secondary shape setting could also be a factor for the different kinetics, as relaxing foams will shift to a lower T_g as relaxation occurs. Additionally, individual foam sample geometry and the rate of water inflow for the sample would have some effect on the kinetics observed both during immersion DMA and expansion experiments. The expansion behavior and volume recovery of unfilled foams matches similar behavior demonstrated with these SMP foams.[4]

The time to expansion correlates to E_{max}; time to 2/3 E_{final} occurred at approximately the final diameter within 10% (~5.5 mm). Volume recovery metrics showing the comparison of time to E_{max}, time to the start of bulk expansion, 2/3 E_{final}, and 90% of the initial bulk diameter are shown in Table II, which demonstrates that the metrics collected could be used for modeling the bulk SMP expansions.

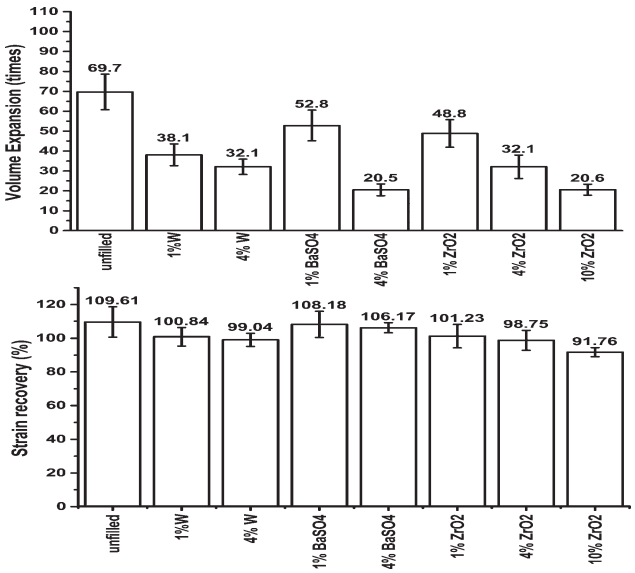

Figure 4. Total volume recovery of bulk samples by immersing crimped samples in 70°C (wet $T_g + 20$°C), showing a decrease in volume recovery with increased loading capacity (top), and the total strain recovery (bottom). The average expansion ratio is shown above the error bars ($n = 9$).

Total volume recovery, performed at approximately 70°C (wet $T_g + 30$°C) for 10 min to determine total actuation behavior, is shown in Figure 4, which also shows the strain recovery. Unfilled foam was found to have volume recovery of approximately 70 times, and swelled to approximately 110% of the original diameter. Additives caused the volume recovery to decrease due to decreased compressibility of the materials. All foams recovered their initial diameters, which compares well with previous examinations of SMP composite materials demonstrating no reduction in recoverable strain with low concentrations of additives.[27,28,47,51,52] The W series showed the most drastic decrease in volume recovery, with 4% W loading having comparable recovery with 10% ZrO_2 loading. The foams were shown to possess high strain recoveries, with all materials demonstrating greater than 90% recoverable strains. Those experiments that showed greater than 100% recovery were due to swelling of the foam materials.

In contrast to other studies that have shown no change in shape memory with higher loading concentrations, these results show a distinct decrease in volume expansion.[2,27,28] This is not synonymous with shape memory, as volume recovery is dependent on the compressed diameter of the material. All materials recovered their initial diameters, but the compressed diameters decreased with higher loading. Based upon the final recovered volumes, the fillers, even at loadings of 10%, did not inhibit the shape recovery of the materials, which is the same as previously published studies.[2,27,28]

Radio-Opacity Enhancement

The X.D. analysis of the materials, appearing in Figure 5 as the raw image and quantitative analysis, indicate that the GDC coils has twice the attenuation of X-rays as the unfilled foam over the monofilament. Quantitatively, the W series displayed the largest enhancement of attenuation for the lowest loading; 4% W loading was observed to have the greatest mean X.D., with 10% ZrO_2 loading possessing the second greatest opacity enhancement. These materials demonstrated substantially superior mean X.D. for both the compressed cylinders of foam and the expanded foam material. Previous studies have commented on the use of radio-opaque additives in SMPs, but do not quantitatively compare additives and commercially available standards.[11,27,28] The expanded foams with the highest loading of each series appeared to have sufficient opacity to appear (visually determined as greater than 0.73 X.D. on the scale used).

An interesting note of this study was that not only were the compressed materials visible during imaging but the materials with higher concentrations were also visible when expanded, as seen in the image in Figure 5. Additionally, GDC coils have been shown to be visible through the skull when used clinically, suggesting that the presented materials would also be visible through tissue.[7–11,53]

CONCLUSIONS

We presented SMP foam chemistry with the addition of three fillers, two of them novel to SMP foams, to determine enhancement of radio-opacity and the effect of the additives on foam properties. Thermal characterization of the materials demonstrated that with addition of fillers, no distinct change in the T_g occurred. Pore size was shown to decrease with increasing additive concentration, with the species of filler altering the change in pore size. The presence of any additive showed an alteration

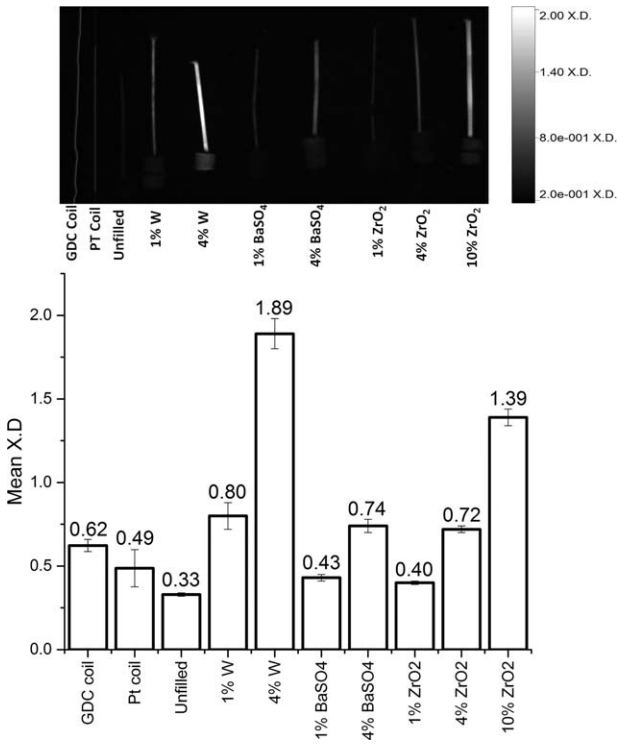

Figure 5. A qualitative (above) and quantitative (below) comparison of the mean X.D. of the crimped 6 mm SMP filled materials and a custom Pt coil compared with a standard GDC device. The normalized average radio-opacity is shown above the error bars, which indicate the standard deviation ($n = 68$).

in pore morphology. Shape recovery kinetics indicated that W filler resulted in delayed time to actuation, determined by both immersion DMA and expansion studies using bulk samples. The time to the start of recovery and time to the approximate final diameters were shown to correlate to the immersion DMA experiments. The use of both bulk material expansions and the immersion DMA experiments is useful in decoupling the geometry of the samples from the response of the materials. Shape recovery showed three main behaviors, with lower concentrations masking the initial delay to expansion. Higher loading of additives led to a delayed actuation initiation period, a fast recovery period, and a slow final recovery to the final diameter. The fillers were also observed to enhance radio-opacity, with 4% W loading displaying the greatest increase. All additives demonstrated an enhancement of opacity, with loading capacities of 4% or higher yielding opacity higher than the vascular device standard GDC coils. Material characteristics such as radio-opacity, shape recovery, and thermal properties need to be understood in order to effectively utilize SMP foam biomaterials in medical devices. The use of these additives could allow for altered times for material expansion and difference in radio-opacity, which could find use in many medical applications.

This work was supported by the National Institutes of Health/National Institute of Biomedical Imaging and Bioengineering Grant R01EB000462, the National Heart Lung and Blood Institute Program of Excellence in Nanotechnology (HHSN268201000046C), and the National Science Foundation (CHE-1410272). The authors thank the Texas A&M University graduate diversity fellowship and Department of Biomedical Engineering for funding. Special thanks to Anthony Boyle for his assistance with volume expansion and editing of the manuscript, and Sayyeda M. Hasaan for foaming advice. The authors acknowledge access to instrumentation within the Laboratory for Synthetic-Biologic Interactions.

REFERENCES

1. Sokolowski, W.; Metcalfe, A.; Hayashi, S.; Yahia, L.; Raymond, J. *Biomed. Mater.* **2007**, *2*, S23.
2. Wache, H.; Tartakowska, D.; Hentrich, A.; Wagner, M. *J. Mater. Sci. Mater. Med.* **2003**, *14*, 109.
3. Wilson, T.; Bearinger, J.; Herberg, J.; Marion, J.; Wright, W.; Evans, C.; Maitland, D. *J. Appl. Polym. Sci.* **2007**, *106*, 540.
4. Singhal, P.; Rodriguez, J.; Small, W.; Eagleston, S.; de Water, J.; Maitland, D.; Wilson, T. *J. Polym. Sci. Part B: Polym. Phys.* **2012**, *50*, 724.
5. Rodriguez, J. N.; Clubb, F. J.; Wilson, T. S.; Miller, M. W.; Fossum, T. W.; Hartman, J.; Tuzun, E.; Singhal, P.; Maitland, D. J. *J. Biomed. Mater. Res. A* **2014**, *102*, 1231.
6. Metcalfe, A.; Desfaits, A. -C.; Salazkin, I.; Yahia, L.; Solokowski, W. M.; Raymond, J. *Biomaterials* **2003**, *24*, 491.
7. Choudhari, K. A.; Flynn, P. A.; McKinstry, S. C. *Neurol. India.* **2007**, *55*, 148.
8. Zubillage, F.; Guglielmi, G.; Vinuela, F.; Duckwiler, G. R. *Am. J. Neuroradiol.* **1994**, *15*, 815.
9. Brisman, J. L.; Song, J. K.; Newell, D. W. *New Engl. J. Med.* **2006**, *355*, 928.
10. Lavine, S. D.; Larsen, D. W.; Giannotto, S. L.; Teitlebaum, G. P. *Neurosurgery* **2000**, *46*, 1013.
11. Rodriguez, J. N.; Yu, Y.; Miller, M. W.; Wilson, T. S.; Hartman, J.; Clubb, F. J.; Gentry, B.; Maitland, D. *J. Ann. Biomed. Eng.* **2012**, *40*, 883.
12. Peuster, M.; Fink, C.; von Schnakenburg, C. *Biomaterials* **2003**, *24*, 4057.
13. Kampmann, C.; Brzezinska, R.; Abidini, M.; Wenzel, A.; Wippermann, C. F.; Habermehl, P.; Knuf, M.; Schumacher, R. *J. Pediatr. Radiol.* **2002**, *32*, 839.
14. Peuster, M.; Fink, C.; Wohlsein, P.; Bruegmann, M.; Gunther, A.; Kaese, V.; Niemeyer, M.; Haferkamp, H.; Schnakenburg, C. V. *Biomaterials* **2003**, *24*, 393.
15. Witten, M. L.; Sheppard, P. R.; Witten, B. L. *Chem. Biol. Interact.* **2012**, *196*, 87.
16. Puester, M.; Kaese, V.; Wuensch, G.; von Schnakenburg, C.; Niemeyer, M.; Fink, C.; Haferkamp, H.; Hausdorf, G. *J. Biomed. Mater. Res. B* **2003**, *65*, 211.
17. Gillani, R.; Ercan, B.; Qiao, A.; Webster, T. *J. Int. J. Nanomed.* **2010**, *5*, 1.
18. Hooy-Corstjens, C. S.; Bulstra, S. K.; Knetsch, M. L. W.; Geusens, P.; Kuijer, R.; Koole, L. H. *J. Biomed. Mater. Res. B* **2007**, *80*, 339.
19. Friedman, C.; Heuer, M.; Rapp, G. *J. Dent. Res.* **1975**, *54*, 921.
20. Moszner, N.; Salz, U. *Macromol. Mater. Eng.* **2007**, *292*, 245.
21. Chithambara Thanoo, B.; Sunny, M. C.; Jayakrishnan, A. *J. App. Biomater.* **1991**, *2*, 67.
22. Kiran, S.; James, N. R.; Jayakrishnan, A.; Joseph, R. *J. Biomed. Mater. Res. A* **2012**, *100*, 3472.
23. Verbeke, F.; Haug, U.; Dhondt, A.; Beck, W.; Schnell, A.; Dietrich, R.; Deppisch, R.; Vanholder, R. *Nephrol. Dial. Transpl.* **2010**, *25*, 1207.
24. Teleflex Incorporated. PTFE-Lined Catheters. **2015**. Available at: https://theinvisiblerisk.org/brands/tfxoem/productAreas/catheters/products/ptfeCatheters/index.html. Accessed on February 16, 2015.
25. Gunes, I.; Cao, F.; Jana, S. *Polymer* **2008**, *49*, 2223.
26. Romero-Ibarra, I.; Bonilla-Blances, E.; Sanchez-Solis, A.; Manero, O. *Eur. Polym. J.* **2012**, *48*, 670.
27. Cui, J.; Lendlein, A. *Smart Mater. Struct.* **2010**, *19*, 1.
28. Cui, J.; Heuchel, M.; Hiebl, B.; Lendlein, A. *Polym. Adv. Technol.* **2009**, *22*, 180.
29. Soghoian, S.; Hoffman, R. S.; Nelson, L. *Am. J. Health Syst. Pharm.* **2010**, *67*, 734.
30. Kelly, J. *Dent. Clin. N. Am.* **2004**, *48*, 513.
31. Piconi, C. *Biomaterials* **1999**, *20*, 1.
32. Dion, I.; Bordenave, L.; Lefebvre, F.; Bareille, R.; Baquey, C.; Monties, J.; Havlik, P. *J. Mater. Sci. Mater. Med.* **1994**, *5*, 18.
33. Cenni, E.; Granchi, D.; Vancini, M.; Pizzoferrato, A. *Biomaterials* **2002**, *23*, 1479.
34. Degidi, M.; Artese, L.; Scarano, A.; Perrotti, V.; Gehrke, P.; Piattelli, A. *J. Periodontol.* **2006**, *77*, 73.

35. Fischer, H.; Luk, M.; Oedekoven, B.; Telle, R.; Mottaghy, K. *J. Biomed. Mater. Res A* **2007**, *81*, 982.

36. Van Oevern, W.; Schoen, P.; Maijers, C. A. *Prog. Biomed. R* **2000**, *5*, 211.

37. Dion, I.; Lahaye, M.; Salmon, R.; Baquey, C.; Monties, J.; Havlik, P. *Biomaterials* **1993**, *14*, 107.

38. De Nardo, L.; Bertoldi, S.; Tanzi, M. C.; Haugen, H. J.; Fare, S. *Smart Mater. Struct.* **2011**, *20*, 035004.

39. Zeugolis, D. I.; Raghunath, M. *Polym. Int.* **2012**, *59*, 1403.

40. Zappa, M. *Mettler Toledo.* **2006**, *2*, 1.

41. He, Z.; Satarkar, N.; Xie, T.; Cheng, Y.; Hilt, J. Z. *Adv. Mater.* **2011**, *23*, 3192.

42. Singhal, P.; Small, W.; Cosgriff-Hernandez, E.; Maitland, D. J.; Wilson, T. *Acta Biomater.* **2014**, *10*, 67.

43. Samouillan, V.; Delaunay, F.; Dandurand, J.; Merbahi, N.; Gardou, J.; Yousfi, M.; Gandaglia, A.; Spina, M.; Lacabanne, C. *J. Funct. Biomater.* **2011**, *2*, 230.

44. Lee, J. M.; Pereira, C. A.; Kan, L. W. K. *J. Biomed. Mater. Res.* **1994**, *28*, 981.

45. Miles, C.; Ghelashvili, M. *Biophys. J.* **1999**, *76*, 3243.

46. Mahfuz, H.; Rangari, V. K.; Islam, M. S.; Jeelani, S. *Compos. A* **2004**, *35*, 453.

47. Wong, J. C. H.; Tervoort, E.; Busato, S.; Ermanni, P.; Gauckler, L. *J. J Colloid Interface Sci.* **2012**, *383*, 1.

48. Salerno, A.; Iannace, S.; Netti, P. A. *Macro. Biosci.* **2008**, *8*, 655.

49. Sauter, T.; Kratz, K.; Lendlein, A. *Macromol. Chem. Phys.* **2013**, *214*, 1184.

50. Sauter, T.; Lutzow, K.; Schossig, M.; Kosmella, H.; Weigel, T.; Kratz, K.; Lendlein, A. *Adv. Eng. Mater.* **2012**, *14*, 818.

51. Ji, H.; Zhong, J.; Meng, J.; Xian, G. *Compos. B* **2013**, *44*, 508.

52. Quadrini, F.; Santo, L.; Squeo, E. A. *Polym. Plast. Technol. Eng.* **2012**, *51*, 560.

53. Piotin, M.; Madai, S.; Sugiu, K.; Gailloud, P.; Rufenacht, D. A. *Am. J. Radiol.* **2002**, *23*, 1580.